Chemical Science

ROYAL SOCIETY OF CHEMISTRY

EDGE ARTICLE

View Article Online
View Journal | View Issue

Cite this: *Chem. Sci.*, 2025, **16**, 19843

All publication charges for this article have been paid for by the Royal Society of Chemistry

Multilevel chirality transfer and second harmonic generation in mesoscopic double helical supramolecular self-assemblies of fullerene enantiomers

Jinrui Li,[a] Kaipeng Zhuang,[a] Yunlong Tao,[b] Qingfeng Zhang, *[b] Hongguang Li *[a] and Jingcheng Hao [a]

Received 18th July 2025
Accepted 9th September 2025

DOI: 10.1039/d5sc05354d

rsc.li/chemical-science

Inducing chirality in the highly symmetric fullerene C_{60} is an effective approach that leads to chiroptical responses over a wide range. However, the optically active expression of C_{60} is a challenging research topic and multiscale modulation of fullerene chirality is still in its infancy. Herein, we synthesized a pair of fulleropyrrolidine enantiomers named R/S-MBA-C_{60} with a monoclinic $P2_1$ chiral space group in the solid-state. Rare mesoscopic double helical supramolecular self-assemblies with distinctly opposite chirality have been obtained. Substantial π–π stacking and non-covalent interactions realize the chirality transfer and amplification across different scales, from the chiral carbon atom to the mesoscopic helix. Such fullerene-based double helical structures exhibit intense CD responses over an extremely wide range, from the UV-visible region and even up to the NIR region, and a SHG effect due the non-centrosymmetric molecular structure. This research develops an efficient approach to precisely modulate fullerene chirality and highlights the potential of chirality-based applications in fullerene science.

Introduction

The demand for chiral nanomaterials with excellent chiroptical properties has been increasing, driven by their potential applications in chiral bio-imaging, spintronics and optoelectronic devices.[1,2] Of great interest are π-conjugated systems with photo- and electroactivities, and diverse topological structures.[3] By modulating the supramolecular interactions of π-conjugated molecules possessing steric elements with other nano-motifs,[4,5] it offers a flexible strategy to tune their chiroptical responses on different scales. Nevertheless, most of them exhibit chiroptical activities mainly in the ultraviolet (UV)-visible region,[6] which may impact practical applications to a certain extent. Thus, chiral nanomaterials possessing chiroptical activity in the far red and possibly NIR regions is highly desired.

Fullerene C_{60} (denoted as C_{60} hereafter) is a unique spherical π-conjugated system, with molar absorption coefficients over an extremely wide wavelength range.[7] Since its discovery in 1985, C_{60} has shown remarkable optical and electrical properties and has become a crucial supramolecular building block.[8] Nevertheless, due to the lack of inherent chirality, the chiral science of C_{60} is still under development.[9] Drawing on the rich chemically modifiable features of fullerenes, even achiral C_{60} can acquire chirality depending on the addends and addition patterns (Table S1),[10–15] exhibiting an excellent chiroptical response.[16–18] For instance, Murata *et al.* reported that an open-cage C_{60} derivative synthesized through a multistep process has a high g_{abs} factor covering the NIR region.[19] Fuchter and co-workers found that bis [60]PCBM shows a fast and high photocurrent response in CPL-detecting devices.[20,21] Moreover, the achiral pristine C_{60} can acquire induced chirality within chiral supramolecular hosts (Table S2),[22–25] resulting in an intense chiroptical signal in the visible region.

Undoubtedly, C_{60}-based π-conjugated structures might constitute a class of chiral optical materials with outstanding performance which are still less explored. Compared to conventional organic chiral molecules, our knowledge on the strategies to hierarchically modulate the chiral response of C_{60} is still limited.[26–28] Very recently, we have found that supramolecular chirality transfer has an impact on the chiroptical properties of pristine C_{60} in the NIR range.[28] Under these circumstances, we maintain scientific skepticism about the relevant behavior of chiral C_{60} derivatives in a similar situation. Considering that second harmonic generation (SHG) is highly sensitive to structural symmetries, we were also interested in exploring the second-order nonlinear optical (NLO) effect of non-centrosymmetric C_{60} derivatives in addition to its chiroptical response.

[a]*Key Laboratory of Colloid and Interface Chemistry, Ministry of Education, School of Chemistry and Chemical Engineering, Shandong University, Jinan 250100, China. E-mail: hgli@sdu.edu.cn*

[b]*College of Chemistry and Molecular Sciences, Wuhan University, Wuhan 430072, China. E-mail: zhangqf@whu.edu.cn*

In the current work, we showcase the synthesis and multi-level chirality transfer in the self-assembly process of fulleropyrrolidine enantiomers. Helical structures with well-defined opposite chirality were obtained by employing the liquid/liquid interfacial precipitation (LLIP) strategy. During this process, chirality transfer and amplification occurred at multiple length scales, which induced intense chiroptical response over a broadband range. The pure enantiomeric assemblies also exhibit efficient SHG responses. Our strategy presented herein features the simple synthesis of chiral C_{60} building blocks, leading to multi-channel responses.

Results and discussion

Synthesis and structural analysis of R/S-MBA-C_{60}

Enantiomers of mono-substituted fulleropyrrolidines named R/S-MBA-C_{60} were synthesized through a one-step thermal reaction (Fig. 1a).[30] Their structures were confirmed by multiple characterization studies (Fig. S1–S5). Single crystals of R/S-MBA-C_{60} were obtained by slow diffusion of MeOH into a stock CS_2 solution at 4 °C. Single crystallographic X-ray diffraction (SCXRD) analysis revealed that both R- and S-MBA-C_{60} crystallized in the $P2_1$ chiral space group with a monoclinic lattice, where the pyrrole-ring attaches to the C_{60} cage at a single [6,6]-bond junction (C1–C2) with a length of 1.60 Å (Fig. 1b).[31] Meanwhile, the purity and homogeneity of R/S-MBA-C_{60} crystals were confirmed by powder X-ray diffraction (PXRD) patterns (Fig. 1c). Thermogravimetric analysis (TGA) showed both enantiomers possess high thermal stabilities up to 174 °C and 180 °C, respectively (Fig. S6). The UV-vis absorption, circular dichroism (CD), and dissymmetry factor g_{abs} spectra of the enantiomers in *o*-xylene are shown in Fig. 1d. The characteristic absorption peak at 430 nm can be attributed to the [6,6]-C_{60} monoadducts (Fig. S7). Obvious mirror-image Cotton effects can be observed over a wide range covering the visible to far-red region (300–750 nm), indicating chiral induction across the whole C_{60} spherical skeleton through its functionalization with a chiral R/S-MBA precursor (Fig. S8 and S9).

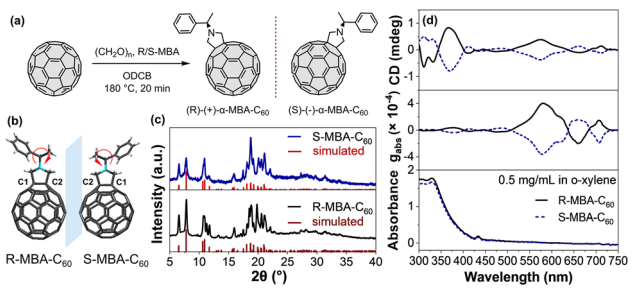

Fig. 1 (a) Reaction of C_{60} with paraformaldehyde and (R/S)-(±)-α-methylbenzylamine (R/S-MBA). (b) Crystal structures of **R-MBA-C_{60}** (left) and **S-MBA-C_{60}** (right), with grey representing C, cyan representing N, and white representing H. (c) Experimental and simulated powder XRD patterns of R/S-MBA-C_{60}. (d) CD, g_{abs}, and UV-vis spectra of the R/S-MBA-C_{60} enantiomers in *o*-xylene (0.5 mg mL^{-1}).

Chirality amplification and supramolecular assembly of mesoscopic helices

Next, we tried to amplify the chirality of individual molecules by triggering the self-assembly of R/S-MBA-C_{60} through a well-known LLIP method in fullerene science.[29,32,33] By placing a poor solvent onto a solution of R/S-MBA-C_{60} in a good solvent, self-assemblies with diverse morphologies could be obtained. By screening various kinds of solvent systems (Fig. S10 and S11), the combination of *o*-xylene/isopropyl alcohol (IPA) was screened. Optimization of the conditions yielded a feed concentration of 1 mg mL^{-1} of R/S-MBA-C_{60} and an incubation time of 72 h, which led to the formation of double helixes with definite opposite supramolecular chirality (Fig. 2a and S12). Obviously, the chirality exhibited by individual C_{60} derivatives was successfully transferred to the supramolecular structure. It should be noted that the use of pure enantiomers is necessary to obtain the helixes, as in a control experiment, only flower-like self-assemblies lacking supramolecular chirality were observed when a racemic mixture (rac-MBA-C_{60}) was used (Fig. S13). This observation highlights the role played by the chiral carbon center during self-assembly.[34]

In the solid state, the as-synthesized R/S-MBA-C_{60} powder shows only random structures (Fig. S14). The path dependence

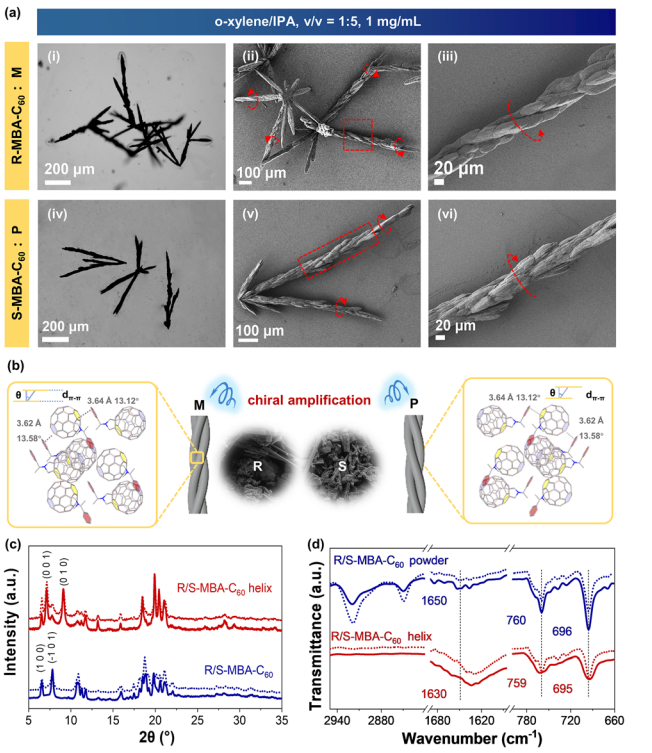

Fig. 2 (a) Micrographs and SEM images of **R-MBA-C_{60}** (i–iii) and **S-MBA-C_{60}** (iv–vi) obtained in a solvent system of *o*-xylene/IPA (v/v = 1 : 5, 1 mg mL^{-1}, incubating for 72 h at 25 °C). (b) The molecular packing mode of R/S-MBA-C_{60} in the helix. The π–π interactions between C_{60}–C_{60} cages are omitted for presentation purposes. The circles denote SEM images of the original R/S-MBA-C_{60} powder. Powder XRD patterns (c), and FT-IR spectra (d) of the R/S-MBA-C_{60} helix. For comparison, curves of pristine powder of R/S-MBA-C_{60} without the LLIP process are also given.

of the helixes indicates that their formation is kinetically controlled. To gain insights into the intermolecular interaction dictating the chirality transfer process, a detailed survey was performed on the composition and inner structure of the self-assemblies. As shown in Fig. 2b and S15, in the crystal packing mode of R/S-MBA-C_{60}, the observed π–π stacking interactions occur between MBA and fullerene units, with vertical plane-to-cage distances of 3.62 Å and 3.64 Å, corresponding to the dihedral angles of 13.58° and 13.12°, respectively.

As illustrated in Fig. 2c, the XRD patterns of such R/S-MBA-C_{60} helixes are subtly different from that of the original powder, although all of them display a monoclinic phase. Substantial π–π interactions and the solvophobic effect induce oriented growth of R/S-MBA-C_{60} in (001) and (010) planes during the self-assembly process. The difference in crystal facet growth rates is precisely the decisive factor in the formation of mesoscale double helical structures, thus realizing the transfer from molecular chirality to supramolecular chirality.[35,36] Combined with the Fourier-transform infrared (FTIR) spectrum (Fig. 2d and S16), both the C=C stretching vibration (1630 cm^{-1}) peak and the characteristic bands of the mono-substituted benzene ring (695 cm^{-1}, 759 cm^{-1}) are red-shifted compared to the pristine powder, again strongly demonstrating the presence of supramolecular interactions in the assemblies, which could be the main reason for their improved thermal stability since they are not solvates, as suggested by thermogravimetric analysis (TGA, Fig. S17).

So far, the mechanism for the apparent chiral amplification trend of the CD signals of the R/S-MBA-C_{60} double helix over the broad wavelength range of 200–800 nm in DRCD spectra (Fig. 3a) has become quite clear. Due to the complexity of the structural features, we further employed dark-field scattering and circular differential scattering (CDS) to measure the optical and chiroptical properties of chiral R/S-MBA-C_{60} helices at the single-particle level. The helix was spin-coated onto clean ITO glass and the corresponding scattering spectra were collected under light excitation using a halogen lamp (Fig. S18). Left/right-handed circular polarized (LCP/RCP) light was generated by adding a quarter-wave plate and polarizer in the optical path. Hyperspectral imaging (Fig. S19) and scattering spectra (Fig. 3b and c) indicate that the R/S-MBA-C_{60} helices tend to scatter light of longer wavelengths and exhibit significant scattering signals between 700 and 790 nm, due to their large size up to several hundred microns.

Meanwhile, the R/S-MBA-C_{60} helices have a higher tendency to scatter chiral light, *i.e.*, the LCP/RCP light. **R-MBA-C_{60}** helix has a stronger scattering ability for LCP between 700 and 750 nm whereas the S-MBA-C_{60} helix exhibits the opposite behavior. The CDS spectra (Fig. 3d) of R/S-MBA-C_{60} helices show nearly perfect mirror-symmetry, which can be obtained by calculating the scattering dissymmetry factor (*g*-factor, see details in the SI).[37–39] While each individual chiral helix exhibits a different spectral line shape, peak position, and intensity of CDS spectra (Fig. S20), averaging more than 20 particles results in CDS spectra that are similar to the ensemble DRCD spectra.

Second-order nonlinear optical effects in mesoscopic helices

Owing to the non-centrosymmetric space group and the chiroptical activity of R/S-MBA-C_{60}, second-order NLO properties are expected. As shown in Fig. S21, a home-built micro-area femtosecond laser system (refer to the SI) was employed to investigate the second harmonic generation (SHG) of the helical

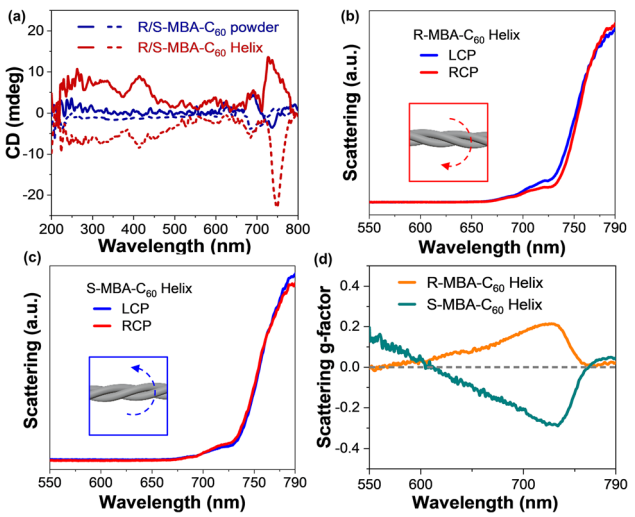

Fig. 3 Chiroptical response of the R/S-MBA-C_{60} helix. (a) Diffuse reflectance circular dichroism (DRCD) spectra of R/S-MBA-C_{60} helices; for comparison, curves of pristine powder of R/S-MBA-C_{60} without the LLIP process are also given. Single-particle scattering spectra of **R-MBA-C_{60}** (b) and S-MBA-C_{60} (c) helices under LCP and RCP excitation. The insets show the corresponding geometric models. LCP/RCP: left/right-handed circularly polarized light. (d) Typical CDS spectra of an individual R/S-MBA-C_{60} helix.

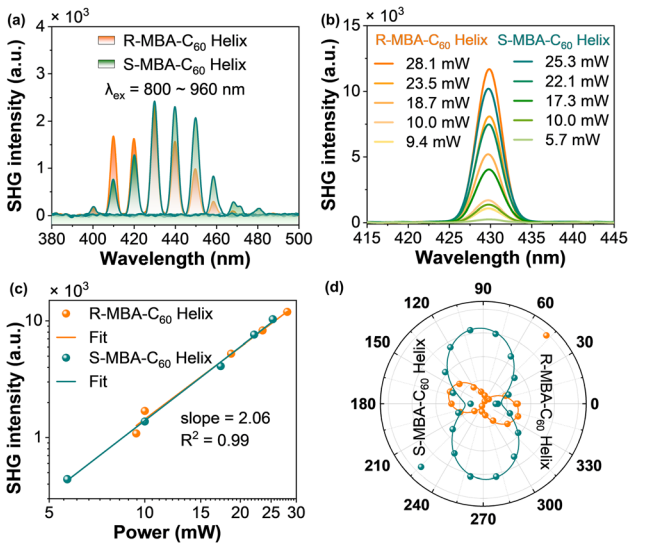

Fig. 4 NLO properties of the R/S-MBA-C_{60} helix. (a) The SHG intensity of R/S-MBA-C_{60} helices pumped with light from 800 nm to 960 nm with a power of 10 mW. (b) SHG spectra of R/S-MBA-C_{60} helices under 860 nm excitation at various powers. (c) Logarithmic plot of the power-dependent SHG intensity under 860 nm excitation. (d) Polarization dependence of the SHG intensity as a function of the linear polarization angle. The solid lines indicate the fitting results.

assemblies. The wavelength-dependent SHG spectra of both R- and S-MBA-C_{60} helixes showed a strong SHG response over a wide wavelength range from 800 to 960 nm, with the strongest SHG intensity at 430 nm under 860 nm excitation (Fig. 4a). Additionally, the results of power-dependent measurements in Fig. 4b confirmed a quadratic dependence of the SHG intensity on the laser power (Fig. 4c) with a slope of about 2, indicating the two-photon nature of the SHG process. To gain further insight into the second-order NLO properties of these chiral helices, polarization dependent measurements were recorded and plotted in a dipolar profile (Fig. 4d), which coincides with a cos4 θ function, showing a dumbbell-shaped fitted curve. The crystal symmetry of R/S-MBA-C_{60} determines the SHG intensity maxima at polarization angles of 160 and 340 deg for **R-MBA-C_{60}**, and of 100 and 280 deg for S-MBA-C_{60}, parallel to the dipolar axis. The polarization ratio, defined as $\rho = (I_{max} - I_{min})/(I_{max} + I_{min})$, was 87.3% and 72.5% for R- and S-MBA-C_{60} helices, respectively, showing high anisotropy with linear polarization. Given that R/S-MBA-C_{60} also shows a photocurrent response (Fig. S22), such multiple-channel properties pave the way for applications in polarization-sensitive optoelectronic prototypes, CPL-sensitive devices and chiral photonics in fullerene science.

Conclusions

In summary, we synthesized a pair of optically active fullerene enantiomers *via* [6,6] addition of chiral functional groups. Mesoscopic double helical assemblies of fullerene with distinctly opposite chirality have been successfully obtained. Substantial π–π stacking and solvophobic effects mediate this rare assembly process, which realizes the chirality transfer and amplification across different scales from the chiral molecule to the mesoscopic helix. Such fullerene-based double helical structures exhibit multiple prominent responses, including chiroptical activity over a wide range, extending even to the NIR region, SHG NLO effects, and polarization-sensitive optoelectronic responses. This work develops an effective approach for precisely modulating fullerene chirality and promotes chirality-based applications in fullerene science.

Author contributions

JRL performed most of the analysis, and led the writing of the manuscript (formal analysis/investigation/methodology/writing). KPZ and YLT contributed to the interpretation of the data (data curation/visualization). QFZ, HGL and JCH improved the text (reviewing/editing).

Conflicts of interest

There are no conflicts to declare.

Data availability

All relevant data are either in the main text or in the SI. Additional data are also available from the authors on request.

CCDC 2414209 (for **R-MBA-C_{60}**) and 2414210 (for **S-MBA-C_{60}**) contain the supplementary crystallographic data for this paper.[40a,b]

Supplementary information: additional experimental details on the synthesis of the chemicals, instrumentation, characterizations, and Fig. S1–S22. See DOI: **https://doi.org/10.1039/d5sc05354d**.

Acknowledgements

This research was made possible by a generous grant from the National Natural Science Foundation of China (Grant Number 21875129 and 22174104). The authors acknowledge the assistance of the Center for Structural and Property Analysis, Core Facilities Sharing Platform, Shandong University.

References

1 F. Furlan, J. M. Moreno-Naranjo, N. Gasparini, S. Feld-mann, J. Wade and M. J. Fuchter, Chiral materials and mechanisms for circularly polarized light-emitting diodes, *Nat. Photonics*, 2024, **1**, 658–665.
2 A. Lininger, G. Palermo, A. Guglielmelli, G. Nicoletta, M. Goel, M. Hinczewski and G. Strangi, Chirality in Light–Matter Interaction, *Adv. Mater.*, 2023, **35**, 2107325.
3 Q. Zhou, W. Yuan, Y. Li, Y. Han, L. Bao, W. Fan, L. Jiao, Y. Zhao, Y. Ni, Y. Zou, H.-B. Yang and J. Wu, [5]Helicene Based π-Conjugated Macrocycles with Persistent Figure-Eight and Möbius Shapes: Efficient Synthesis, Chiral Resolution and Bright Circularly Polarized Luminescence, *Angew. Chem., Int. Ed.*, 2025, **64**, e202417749.
4 K. E. Ebbert, E. Benchimol, A. Platzek, C. Drechsler, J. Openy, S. Hasegawa, J. J. Holstein and G. H. Clever, Ring-Size Control and Guest-Induced Circularly Polarized Luminescence in Heteroleptic $Pd_3A_3B_3$ and $Pd_4A_4B_4$ Assemblies, *Angew. Chem., Int. Ed.*, 2024, **63**, e202413323.
5 S. Di Noja, F. Amato, F. Zinna, L. Di Bari, G. Ragazzon and M. Prato, Transfer of Axial Chirality to the Nanoscale Endows Carbon Nanodots with Circularly Polarized Luminescence, *Angew. Chem., Int. Ed.*, 2022, **61**, e202202397.
6 X. Xiao, S. K. Pedersen, D. Aranda, J. Yang, R. A. Wiscons, M. Pittelkow, M. L. Steigerwald, F. Santoro, N. J. Schuster and C. Nuckolls, Chirality Amplified: Long, Discrete Helicene Nanoribbons, *J. Am. Chem. Soc.*, 2021, **143**, 983–991.
7 Y. Segawa, H. Ito and K. Itami, Structurally uniform and atomically precise carbon nanostructures, *Nat. Rev. Mater.*, 2016, **1**, 15002.
8 X. Chang, Y. Xu and M. von Delius, Recent advances in supramolecular fullerene chemistry, *Chem. Soc. Rev.*, 2024, **53**, 47–83.
9 C. Thilgen and F. Diederich, Structural Aspects of Fullerene Chemistry–A Journey through Fullerene Chirality, *Chem. Rev.*, 2006, **106**, 5049–5135.
10 N. Chronakis, U. Hartnagel, M. Braun and A. Hirsch, A chiral dumbbell shaped bis(fullerene) oligoelectrolyte, *Chem. Commun.*, 2007, **6**, 607–609.

11 E. E. Maroto, S. Filippone, M. Suárez, R. Martínez-Álvarez, A. de Cózar, F. P. Cossío and N. Martín, Stereodivergent Synthesis of Chiral Fullerenes by [3 + 2] Cycloadditions to C_{60}, *J. Am. Chem. Soc.*, 2014, **136**, 705–712.
12 N. Ousaka, F. Mamiya, Y. Iwata, K. Nishimura and E. Yashima, "Helix-in-Helix" Superstructure Formation through Encapsulation of Fullerene-Bound Helical Peptides within a Helical Poly(methyl methacrylate) Cavity, *Angew. Chem., Int. Ed.*, 2017, **56**, 791–795.
13 M. Wachter, L. Jurkiewicz and A. Hirsch, Sequential Tether-Directed Synthesis of New [3 : 2 : 1] Hexakis-Adducts of C_{60} with a Mixed Octahedral Addition Pattern, *Chem.–Eur. J.*, 2021, **27**, 7677–7686.
14 S. Filippone, E. Maroto, Á. Martín-Domenech, M. Suarez and N. Martín, An efficient approach to chiral fullerene derivatives by catalytic enantioselective 1,3-dipolar cycloadditions, *Nat. Chem.*, 2009, **1**, 578–582.
15 E. Maroto, M. Izquierdo, S. Reboredo, J. Marco-Martínez, S. Filippone and N. Martín, Chiral Fullerenes from Asymmetric Catalysis, *Acc. Chem. Res.*, 2014, **47**, 2660–2770.
16 Z. Lu, T. K. Ronson, A. W. Heard, S. Feldmann, N. Vanthuyne, A. Martinez and J. R. Nitschke, Enantioselective fullerene functionalization through stereochemical information transfer from a self-assembled cage, *Nat. Chem.*, 2022, **15**, 405–412.
17 Y. Hashikawa, S. Okamoto and Y. Murata, Synthesis of inter-[60]fullerene conjugates with inherent chirality, *Nat. Commun.*, 2024, **15**, 514.
18 Y. Hashikawa, S. Okamoto, S. Sadai and Y. Murata, Chiral Open-[60]Fullerene Ligands with Giant Dissymmetry Factors, *J. Am. Chem. Soc.*, 2022, **144**, 18829–18833.
19 Y. Hashikawa, S. Sadai, S. Okamoto and Y. Murata, Near-Infrared-Absorbing Chiral Open [60]Fullerenes, *Angew. Chem., Int. Ed.*, 2023, **135**, e202215380.
20 W. Shi, F. Salerno, M. D. Ward, A. Santana-Bonilla, J. Wade, X. Hou, T. Liu, T. J. S. Dennis, A. J. Campbell, K. E. Jelfs and M. J. Fuchter, Fullerene Desymmetrization as a Means to Achieve Single-Enantiomer Electron Acceptors with Maximized Chiroptical Responsiveness, *Adv. Mater.*, 2021, **33**, e2004115.
21 W. Shi, Q. Zhuang, R. Zhou, X. Hou, X. Zhao, J. Kong and M. J. Fuchter, Enantiomerically Pure Fullerenes as a Means to Enhance the Performance of Perovskite Solar Cells, *Adv. Energy Mater.*, 2023, **13**, 2300054.
22 J. Kou, Q. Wu, D. Cui, Y. Geng, K. Zhang, M. Zhang, H. Zang, X. Wang, Z. Su and C. Sun, Selective Encapsulation and Chiral Induction of C_{60} and C_{70} Fullerenes by Axially Chiral Porous Aromatic Cages, *Angew. Chem., Int. Ed.*, 2023, **62**, e202312733.
23 S. W. Lo, T. Kitao, Y. Nada, K. Murata, K. Ishii and T. Uemura, Chiral Induction in Buckminsterfullerene Using a Metal–Organic Framework, *Angew. Chem., Int. Ed.*, 2021, **60**, 17947–17951.
24 A. Jozeliunaitė, A. Neniškis, A. Bertran, A. M. Bowen, M. Di Valentin, S. Raišys, P. Baronas, K. Kazlauskas, L. Vilčiauskas and E. Orentas, Fullerene Complexation in a Hydrogen-Bonded Porphyrin Receptor via Induced-Fit: Cooperative Action of Tautomerization and C–H$\cdots\pi$ Interactions, *J. Am. Chem. Soc.*, 2022, **145**, 455–464.
25 M. Yamamura, T. Saito, T. Hasegawa, E. Nishibori and T. Nabeshima, Synthesis of a chiral metallo-capsule composed of concave molecules and chirogenesis upon fullerene binding, *Chem. Commun.*, 2021, **57**, 8754–8757.
26 Y. Hizume, K. Tashiro, R. Charvet, Y. Yamamoto, A. Saeki, S. Seki and T. Aida, Chiroselective Assembly of a Chiral Porphyrin-Fullerene Dyad: Photoconductive Nanofiber with a Top-Class Ambipolar Charge-Carrier Mobility, *J. Am. Chem. Soc.*, 2010, **132**, 6628–6629.
27 A. J. Hilmer, D. O. Bellisario, S. Shimizu, T. P. McNicholas, Q. H. Wang, S. A. Speakman and M. S. Strano, Formation of High-Aspect-Ratio Helical Nanorods via Chiral Self-Assembly of Fullerodendrimers, *J. Phys. Chem. Lett.*, 2014, **5**, 929–934.
28 A. Insuasty, C. Atienza, J. Luis López and N. Martín, Supramolecular pentapeptide-based fullerene nanofibers: effect of molecular chirality, *Chem. Commun.*, 2015, **51**, 10506–10509.
29 J. Li, Y. Bi, Z. Liu, Z. Yang, X. Xin, L. Feng, H. Li and J. Hao, Chiral metal nanocluster within nanoarchitecture of fullerene C_{60}: Chirality transfer and improvement of nonlinear optical property, *Nano Res.*, 2024, **17**, 9255–9260.
30 Y. Li, D. Zhang, H. Wang, F. Li, L. Sun, L. Liu, C. Liu, A. M. Asiri and K. A. Alamry, Metal-Free Synthesis of N-Alkyl-2,5-Unsubstituted/Monosubstituted Fulleropyrrolidines: Reaction of [60]Fullerene with Paraformaldehyde and Amines, *J. Org. Chem.*, 2019, **84**, 2922–2932.
31 Deposition numbers 2414209 (for **R-MBA-C_{60}**) and 2414210 (for **S-MBA-C_{60}**) contain the supplementary crystallographic data for this paper. These data are provided free of charge by the joint Cambridge Crystallographic Data Centre and Fachinformationszentrum Karlsruhe Access Structures service.
32 J. Li, K. Zhuang, Y. Mao, C. Liu, M. Pang and H. Li, Nanoarchitectonics of mesoporous carbon from C_{60}/PCBM hybrid crystals for supercapacitor, *Carbon*, 2023, **201**, 449–459.
33 S. Maji, L. K. Shrestha and K. Ariga, Nanoarchitectonics for Hierarchical Fullerene Nanomaterials, *Nanomaterials*, 2021, **11**, 2146.
34 M. Fortino, A. Mattoni and A. Pietropaolo, The role of metal-halide bond in the distortions and asymmetric non-covalent interactions in chiral hybrid perovskites, *J. Phys. Mater.*, 2024, **7**, 045009.
35 P. Wu, A. Pietropaolo, M. Fortino, S. Shimoda, K. Maeda, T. Nishimura, M. Bando, N. Naga and T. Nakano, Non-uniform Self-folding of Helical Poly(fluorenevinylene) Derivatives in the Solid State Leading to Amplified Circular Dichroism and Circularly Polarized Light Emission, *Angew. Chem., Int. Ed.*, 2022, **61**, e202210556.
36 A. R. A. Palmans and E. W. Meijer, Amplification of Chirality in Dynamic Supramolecular Aggregates, *Angew. Chem., Int. Ed.*, 2007, **46**, 8948–8968.

37 Q. Zhang, T. Hernandez, K. W. Smith, S. A. H. Jebeli, A. X. Dai, L. Warning, R. Baiyasi, L. A. McCarthy, H. Guo, D. Chen, J. A. Dionne, C. F. Landes and S. Link, Unraveling the origin of chirality from plasmonic nanoparticle-protein complexes, *Science*, 2019, **365**, 1475–1478.

38 J. Wan, L. Sun, X. Sun, C. Liu, G. Yang, B. Zhang, Y. Tao, Y. Yang and Q. Zhang, Cu^{2+}-Dominated Chirality Transfer from Chiral Molecules to Concave Chiral Au Nanoparticles, *J. Am. Chem. Soc.*, 2024, **146**, 10640–10654.

39 X. Sun, L. Sun, L. Lin, S. Guo, Y. Yang, B. Zhang, C. Liu, Y. Tao and Q. Zhang, Tuning the Geometry and Optical Chirality of Pentatwinned Au Nanoparticles with 5-Fold Rotational Symmetry, *ACS Nano*, 2024, **18**, 9543–9556.

40 (*a*) J. Li K. Zhuang Y. Tao Q. Zhang H. Li and J. Hao, CCDC 2414209: Experimental Crystal Structure Determination, 2025, DOI: **10.5517/ccdc.csd.cc2m15ql**.; (*b*) J. Li K. Zhuang Y. Tao Q. Zhang H. Li and J. Hao, CCDC 2414210: Experimental Crystal Structure Determination, 2025, DOI: **10.5517/ccdc.csd.cc2m15rm**.